Theoretical elements for the design of a small scale Linear Fresnel Reflector: Frontal and lateral views

A. Barbón [a], N. Barbón [a], L. Bayón [b,*], J.A. Otero [b]

[a] *EPI, Department of Electrical Engineering, University of Oviedo, Gijón, Spain*
[b] *EPI, Department of Mathematics, University of Oviedo, Gijón, Spain*

Communicated by: Associate Editor Jayanta Kumar Nayak

Abstract

This paper addresses the problem of the mathematical design of a Linear Fresnel Reflector, specifically the design of a reflector concentrator with flat mirrors and a single absorber tube. The mathematical aspects of the design, i.e., the number, width and position of the primary mirrors and the height, length and relative position of the single absorber tube, are analysed. The optimization of the relative position with respect to the primary reflectors and the size of the single absorber tube are both addressed, further analysing up to 12 different configurations. To do so, both the frontal and lateral view of the structure are taken into account. The lateral optical performance factor analysed here, has been overlooked until now, as it may be insignificant in large-scale concentrators. It is shown in this paper that it is a key aspect in medium- and small-scale concentrators, the most common in applications in the Household Sector like, for example, micro-cogeneration. Finally, a number of numerical simulations performed in a custom-designed program compiled using Mathematica® is presented. At the time of this writing, a prototype is being built at CIFP in La Felguera, Asturias, Spain.
© 2016 Elsevier Ltd. All rights reserved.

1. Introduction

Concentrated Solar Power (CSP) is called to play a very important role in future energy sources. There are many possible configurations for CSP, such as the parabolic dish, linear Fresnel, parabolic trough and central receiver. Linear Fresnel Reflectors (LFRs) are still much less popular than Parabolic Trough Concentrators (PTCs) for concentrated solar applications. The main disadvantage of LFRs compared to PTCs is that the concentration factor achieved to date is notably lower. Moreover, this factor varies notably during the day. In recent years, however,

LFRs have become an attractive option to generate electricity from solar radiation. LFRs present certain advantages in the field of concentrating solar power because of their simplicity, robustness and low capital cost. Apart of prototypes, there are already two commercial LFR plants for power generation: Kimberlina (5 MW), in California (USA); and Puerto Errado 2 (30 MW), in Spain. The latter has been in service since August 2012 (Novatec, 2015). In addition to the aforementioned plants, there is also a Fresnel plant that provides saturated steam to a power station in Liddell (Australia). The reader can find a review of different linear Fresnel collector designs in Montes et al. (2014). All existing LFR plants use water-steam as the heat transfer fluid. However, there are also studies that analyse the behaviour of other fluids. For example, molten nitrates

* Corresponding author.
E-mail address: bayon@uniovi.es (L. Bayón).

are proposed as the heat transfer fluid in a LFR in Grena and Tarquini (2011).

From the point of view of the design of the concentrator, there are basically two types of Fresnel lens solar concentrators: point focusing Fresnel lens concentrators, based on refraction lenses, which are used for high temperature applications (e.g., concentrated solar power generation); and line focusing Fresnel lens concentrators, based on reflection mirrors, which are used for mid-temperature applications such as solar cooling, steam generation and industrial process heat. This paper deals with the latter type: the Linear Fresnel Reflector Concentrator.

From the point of view of the movement of the LFR, two types of LFR systems have been reported in the literature (see Sharma et al., 2015). In the first type (I), the individual reflector-rows are kept fixed and the reflectors-receiver system is tracked so as to follow the apparent movement of the sun. In the second type (II), the receiver remains stationary and the reflector-rows are tracked so as to follow the sun's movement. In this paper, we analyse the type-II LFR, adapting a well-known method (Mathur et al., 1991a,b) that, until now, has been applied up for type-I LFRs. The version of the method we present here enables us to avoid the effect of shading and blocking.

Different LFR configurations have been proposed in the literature: the "conventional" central LFR, with a single absorber in the centre of the array of mirrors and a compact linear Fresnel concentrator (CLFC). The CLFC (Mills and Morrison, 2000) consists in installing a linear absorber at each side of the mirror array so that consecutive mirrors point to different absorbers. This arrangement minimizes beam blocking between adjacent reflectors. An interesting comparative analysis of central LFRs and CLFCs is presented in Montes et al. (2014). Other papers focus on the cost of the design. An economic comparison of PTCs and LFRs is made in Morin et al. (2012). In Nixon and Davies (2012), the cost factor to be minimized is the ratio of the capital cost per exergy (available power output). Receiver orientations may be horizontal, vertical or inclined, with many possible configurations for the Fresnel receiver model being reported in the literature. Two linear receivers on separate towers with double row tube arrangements of branch tubes are considered in Mills and Morrison (2000). A multitube Fresnel receiver is presented in Abbas et al. (2012b), the receiver consisting of a bundle of tubes parallel to the mirror arrays. Four trapezoidal cavity absorbers for LFRs are compared in Singh et al. (2010), while a LFR with a V-shaped cavity receiver was studied in Lin et al. (2013). As to the shape of the mirrors, we shall consider flat mirrors in this paper, although other types can be found in the literature. For example, Abbas et al. (2012a), analyse the use of different optical designs, including circular-cylindrical and parabolic-cylindrical mirrors with different reference positions.

As already stated, in addition to the Linear Fresnel mirror reflector, devices with a Fresnel refraction lens are also used (Xie et al., 2011b; Zhai et al., 2010). In these cases, the Fresnel lens is manufactured using simple plastics such as polymethylmethacrylate which achieve a transmissivity of nearly 0.93. An optimum convex shaped non-imaging Fresnel lens is designed in Leutz et al. (1999). Lin et al. (2014), analysed the optical and thermal performance of four types of cavity receiver (triangular, arc-shaped, rectangular and semi-circular). Xie et al. (2011a), provides an excellent review of recent developments (from 1951 to 2011) using different types of Fresnel lenses, with more than 100 references. With regard to the types of studies carried out, there are also several (non-exclusive) possibilities: optical design (Montes et al., 2014), economic study (Nixon and Davies, 2012) and analysis of thermal performance (Singh et al., 2010). There are many papers of this last type which analyse heat transfer processes, some of which have been developed using Engineering Equation Solver (EES).

This paper addresses neither the thermal performance nor the economic aspects of LFRs; rather, we focus on the mathematical design of an optimal configuration. When designing a LFR plant, the following aspects need to be taken into account: mirror width, tracking system design, curvature of the mirrors (flat, circular or parabolic), average concentration ratio, height of the receiver above the primary mirrors and receiver design (multiple tube or single-tube). This paper focuses on the mathematical aspects of the design, i.e., the number, width and position of the primary mirrors and the height, length and relative position of the receiver.

For the sake of simplicity, we assume flat mirrors and a single absorber tube. Moreover, the design of the secondary reflector will not be taken into consideration. Specifically, we shall optimize the size and relative position of the single absorber tube with respect to the primary reflectors, analysing up to 12 different configurations. To do so, we shall consider both the frontal and lateral view of the structure. The lateral optical performance presented in this paper has been overlooked until now, as it may be insignificant in large-scale concentrators. As we shall see, however, it is a key aspect in medium- and small-scale concentrators, the most common in the Household Sector. Very few authors use the LFR for heating and sanitary hot water. It should be borne in mind that the Household Sector represents the largest energy use in Europe, more so even than Industry, consuming 26.2% of the EU total final energy in 2012 (Fetie, 2014). Obviously, not all countries offer the same possibilities for harnessing solar energy. In Europe, the Alps and the adjacent mountain ranges form the natural border between the sunny south and the more diffuse north. Very comprehensive information on the potential of solar energy in the European Union can be found in Suri et al. (2007). Moreover, using the LFR for heating water for its direct use removes the large losses due to electric transformation, of around 40%. For these reasons, we consider it necessary to carry out a study of the use of LFR technology in the Household Sector.

This paper is the starting point for an in-depth analysis of various aspects of small-scale Linear Fresnel Reflectors (LFRs). We highlight two main contributions:

(i) A detailed study of the lateral behaviour of the LFR. In large scale LFRs, this study is not usually performed for two reasons. First, the size of the absorber does not permit any configuration allowing the modification of its position. Second, the influence of the lateral position can be considered irrelevant in % terms with respect to the total length of the absorber. In small-scale LFRs of small size, however, like those analyzed in this paper, this study is an essential prerequisite. We show how, the omission of this study in small-scale LFRs leads to important design errors in some cases.

(ii) A novel mathematical modelization of the mirror field width (M_{fw}). This parameter is fundamental in the installation of small scale LFRs in urban residential buildings. In most of the studies, the area of the primary reflector, A_{pm}, remains constant, due to the available surface in the roof of the building is the first input variable. To perform the design of the installation, the aspect ratio for the LFR, defined as the ratio between M_{fw} and the length of the mirrors L_M in the primary reflector, is used. With the aid of the results obtained for the mirror field width (M_{fw}), this study will be feasible.

The paper is organized as follows. In Section 2, we present the nomenclature used in the paper. Section 3 presents the frontal design, which is the most usual design. Adapting Mathur's method, we have designed a type-II LFR that enables the effects of shading and blocking to be avoided. First, our study is based on the assumption that the incident light rays are parallel. Subsequently, due to the finite angular size of the sun's disc, we generalize the study considering the sun's rays reaching the absorber tube to be non-parallel. In Section 4, we present the novel lateral design, analysing a number of configurations. The parameters that allow us to conduct a comparative analysis of the suggested configurations is presented in Section 5. Several numerical simulations are presented in Section 6. Despite the fact that several commercial programs are available, we have preferred to develop our own program compiled in Mathematica®. Finally, Section 7 summarizes the main contributions and conclusions of the paper, as well as outlining future perspectives.

2. Nomenclature

λ	latitude angle (°)
L	longitude angle (°)
L_0	L of observer's meridian (°)
L_{UTC}	L of time zone's meridian (°)
γ_S	height angle of the sun (°)
θ_z	zenith angle of the sun (°)
α_S	azimuth of the sun (°)
ω	hour angle (°)
T_S	solar time (h)
ET	time equation (h)
Γ	day angle (°)
n_d	ordinal of the day
T_L	legal time (h)
T_{UTC}	UTC time (h)
A_H	daylight saving time (h)
δ	solar declination (°)
$-\omega_s$	angle of sunrise (°)
ω_s	angle of sunset (°)
θ_f	frontal incidence angle (°)
θ_l	angle between the zenith and the projection of solar rays onto the NS plane (°)
W	width of the mirrors (m)
f	height of the receiver (m)
n	number of mirrors at each side of the central mirror
L_i	position of i-th mirror ($0 \leqslant i \leqslant 2n$) (m)
L_i^l	L_i of the left side ($1 \leqslant i \leqslant n$) (m)
L_i^r	L_i (right side) (m)
β_i	tilt of i-th mirror (°)
β_i^l	β_i (left side) (°)
β_i^r	β_i (right side) (°)
$\overline{\beta}_n^l$	β_n^l for $\theta_f = 45°$ (°)
ξ	aperture of solar rays (9.30 mrad)
W_a	width of the absorber (m)
r_c	width of the image produced on the flat absorber by the last mirror on the left side (m)
r_l	width to the left on the flat absorber, due to considering ξ (m)
r_r	width to the right on the flat absorber, due to considering ξ (m)
α_i	angle between the vertical at the focal point and the line connecting the centre point of each mirror to the focal point (°)
W_{ai}	width illuminated on the absorber by the i-th mirror (m)
W_a^*	minimum value of W_{ai} for $0 \leqslant i \leqslant 2n$ (m)
D	diameter of the absorber tube (m)
L_{ai}	length of the circumference illuminated on the absorber by the i-th mirror (m)
θ_i	angle between the normal to the mirror and the angle of incidence of the sun (°)
θ_{ai}	angle between the normal to the absorber and the reflected ray (°)
H_i', H_i''	auxiliary parameters for the study of non-parallel rays (m)
d_i'	width illuminated to the left on the tube of the absorber, due to considering ξ (m)
d_i''	width illuminated to the right on the tube of the absorber, due to considering ξ (m)
L_M	length of the mirrors (m)

y_i	auxiliary parameters of the lateral design ($i = 1, 2, 3, 4$) (m)
x_i	auxiliary parameters of the lateral design ($i = 1, 2, 3, 4$) (m)
x_0, x_f	auxiliary parameters of the lateral design (m)
μ	angle between the reflected ray and the normal to the NS axis (°)
θ_L	lateral incidence angle (°)
ζ	the angle θ_z for day $n_d = 195$ and for solar time $T_S = 12$ ($\zeta = 21.47°$)
$\eta_{optical}$	optical efficiency (%)
η_{energy}	energy efficiency (%)
ρ_m	reflectivity of the primary mirrors
E_{ir}	incident energy on the receiver (W)
DNI	Direct Normal Irradiance (W/m^2)
A_{pm}	area of the primary reflectors (m^2)
CR	concentration ratio
A_{abs}	area of the single absorber tube (m^2)
L_{abs}	length of the single absorber tube (m)
L_M	length of mirrors in the primary reflector (m)
CR_r	real concentration ratio
l_a^l	left illuminated length of the single absorber tube (m)
l_a^r	right illuminated length of the single absorber tube (m)
l_a^T	total illuminated length of the single absorber tube (m)
LR	length ratio
D_e	deviation with respect to the vertical of the single absorber tube (m)
R	incident radiation, with $|R| = 1$
R_l	lateral component of R
R_{fi}	frontal component of R
R_i	resultant of the incident radiation
R_i'	R_i take into account the incidence cosines
R_i^{sim}	the common simplification of R_i'
r_W	ratio of widths
M_{fw}	mirror field width (m)

Considering a LFR aligned horizontally and aligned in a North–South orientation (see Figs. 1 and 2), the angle of incidence of solar radiation will be calculated in two projection planes: the frontal incidence angle, θ_f, and the lateral incidence angle, θ_l. The former, θ_f, is defined as the angle between the vertical and the projection of the sun vector
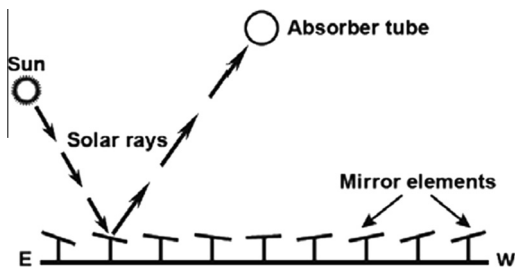

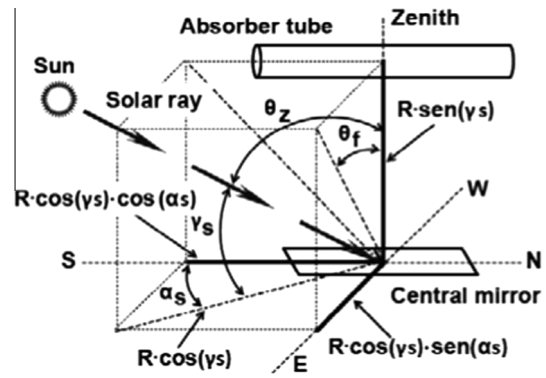Fig. 1. Sketch of a LFR. Frontal view.

Fig. 2. Basic definitions. Lateral view.

on the EW plane (the plane orthogonal to the absorber tube), while θ_l is defined as the angle between the vertical and the projection of the sun vector on the NS plane.

3. Frontal design

The frontal design of the LFR has been studied by several authors (an excellent summary can be found in Sharma et al., 2015). In this paper, we use a method inspired by what is known as 'Mathur's method' (Mathur et al., 1991a,b), which calculates the appropriate value of the shift between adjacent mirrors such that shading and blocking of reflected rays are avoided. The method (Mathur et al., 1991a,b) considers the concentrator in the type-I LFR to be perfectly tracked and that the ray coming from the centre of the solar disc is perpendicular to the concentrator aperture. Let us now see how to adapt this method to the study of a type-II LFR so that the effects of shading and blocking can be avoided.

Due to the linearity of LFRs, in this section all optical properties are defined in the transversal plane, i.e., the plane normal to the longitudinal rotation axes of the mirrors. These axes are parallel to the single-tube receiver.

The performance of LFRs is based on properly selecting the number of mirrors, the width of the mirrors (W), the separation between two consecutive mirrors, i.e., the position of each mirror (L_i) with respect to the central mirror ($i = 0$), the tilt of each mirror (β_i), and the height of the receiver (f). In this part of the study, we assume that a flat absorber of appropriate size will be placed in the focal plane of the LFR, although we shall later calculate its optimal size. A sketch of the mirror field of the LFR employing mirror elements of equal width and using a flat horizontal absorber with a NS design on the left-hand-side of an absorber tube is presented in Fig. 3.

3.1. Position of the primary reflectors

The tilt (or reference position) of each mirror (β_i) was adjusted so that the incident ray (which arrives at an angle θ_f) reaches the focal point after a single reflection. The focal plane is located at a distance f from the reflecting element placed in the centre of the LFR ($L_0 = 0$). The pivoting
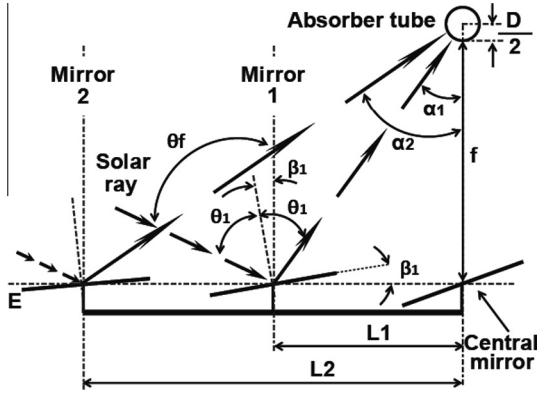
Fig. 3. Definitions used in the frontal design.

point of each mirror coincides with the central point of the mirror; hence, it is always focused on the central point of the receiver.

An appropriate distance (shift) must be kept between two consecutive mirrors so that a mirror does not shade its adjacent mirror element. Each mirror may thus be characterized by two parameters: position (L_i), and tilt (β_i). To calculate these parameters, we distinguish between: the central mirror ($i = 0$), the mirrors to the left ($1 \leqslant i \leqslant n$) and those to the right ($1 \leqslant i \leqslant n$). Hence, the total number of mirrors of the LFR is: $2n + 1$.

To calculate the reference position, as the sun moves in the projection plane, the mirrors must rotate around their axes in such a way that the above principle is fulfilled. The following expressions were used to obtain these parameters using simple geometrical optics:

$$\beta_i^l = \frac{1}{2} \arctan \left[\frac{L_{i-1}^l}{f} + \frac{W}{2f} \left[\frac{\sin \beta_{i-1}^l + \sin \beta_i^l}{\tan(90° - \theta_f - \xi/2)} + \cos \beta_{i-1}^l \right. \right.$$
$$\left. \left. + \cos \beta_i^l \right] \right] + \frac{\theta_f}{2} \tag{1}$$

$$L_i^l = L_{i-1}^l + \frac{W}{2} \left[\frac{\sin \beta_{i-1}^l + \sin \beta_i^l}{\tan(90° - \theta_f - \xi/2)} + \cos \beta_{i-1}^l + \cos \beta_i^l \right] \tag{2}$$

where ξ is the natural aperture of solar radiation (about $64' = 9.30$ mrad), $1 \leqslant i \leqslant n$, and n is the number of mirrors on the left side of the LFR. This set of equations are modified versions of those found in Mathur et al. (1991a,b). Other variations of these formulas can be found in Singh et al. (2010) and Nixon and Davies (2012).

Eqs. (2) and (1) are solved iteratively ($1 \leqslant i \leqslant n$) and the following are considered the initial conditions of the central mirror at 9:00 am ($\theta_f = 45°$):

$$L_0^l = 0; \quad \beta_0^l = 22.5° \tag{3}$$

Assuming the LFR to perform symmetrically throughout the day, the spacing between the reflecting elements on the right side is the same as that on the left side of the LFR:

$$L_i^r = L_i^l = L_i \tag{4}$$

while the determination of the tilt, β_i^r, on the right side is given by:

$$\beta_i^r = \frac{\theta_f - \arctan \left[\frac{L_i}{f} \right]}{2}; \quad 1 \leqslant i \leqslant n \tag{5}$$

For the sake of convenience, we consider β_i^l, $\beta_i^r > 0$ if they are measured counter-clockwise above the horizontal axis.

3.2. Width of a single absorber tube

Two approaches may be used to determine the width of the flat horizontal absorber (W_a).

(1) One (Mathur et al., 1991a,b) is to consider the last element on the left side of the LFR, with maximum tilt in the operating period, $\overline{\beta}_n^l$ (i.e., β_n^l for $\theta_f = 45°$), as it is the element that will provide the widest image on the receiver plane. If we design the width of the absorber so that this image is covered by it, we have that:

$$W_a = r_l + r_c + r_r \tag{6}$$

where r_c is the width of the image produced on the flat absorber by the aforementioned last mirror. Likewise, r_l and r_r respectively represent the width produced to the left and the right, in the case of considering ξ, the natural aperture of solar radiation. Operating straightforwardly, we thus have that:

$$r_c = W \cos \overline{\beta}_n^l + W \sin \overline{\beta}_n^l \tan \left(\arctan \frac{L_n}{f} \right) \tag{7}$$

$$r_l = \left(f - \frac{W}{2} \sin \overline{\beta}_n^l \right) \left[\tan \left(\arctan \frac{L_n}{f} \right) \right.$$
$$\left. - \tan \left(\arctan \frac{L_n}{f} - \xi/2 \right) \right] \tag{8}$$

$$r_r = \left(f + \frac{W}{2} \sin \overline{\beta}_n^l \right) \left[\tan \left(\arctan \frac{L_n}{f} + \xi/2 \right) \right.$$
$$\left. - \tan \left(\arctan \frac{L_n}{f} \right) \right] \tag{9}$$

As can be seen, if we neglect the effect of ξ, we have that $r_l = r_r = 0$. This approach has the serious drawback that the absorber is totally covered at only one time of the day. For these reasons, we shall propose a second design choice in this paper.

(2) A second approach is to determine the optimum width in order to ensure that the absorber is covered at all times of the day. If we denote by α_i the angle between the vertical at the focal point and the line connecting the centre point of each mirror to the focal point (see Fig. 3), and denote by β_i the tilt angle of any mirror (i.e., we merge β_i^l and β_i^r), it can be shown that the width of the absorber in this case is given by the following formula:

$$W_{ai} = W[\cos \beta_i \pm \sin \beta_i \tan \alpha_i]; \quad 0 \leqslant i \leqslant 2n \tag{10}$$

which, as can be seen, depends on each mirror, and where the sign $\pm$ must be adopted according to the following criteria: $-$ for the left side, and $+$ for the right side.

In this study, we have considered the latter option to be far better; although there are times when the sun's rays fall outside the single absorber tube, it is precisely there where the design of the secondary reflector must play a decisive role. The design value that we shall consider is:

$$W_a^* = \min_{0 \leqslant i \leqslant 2n} W_{ai} \qquad (11)$$

a value which means that the entire absorber will always be illuminated. We shall see the results obtained in the different simulations in Section 6. The reader will have noticed that, for the sake of simplicity, up until now we have considered a flat absorber. However, our design will use cylindrical tubes, whose diameter (D) will be one of the key factors in the design. For this reason and to conclude the frontal study, let us now see the equivalent formulas to (10) to use in the case of a cylindrical absorber.

If we denote by L_{ai} the length of the circumference illuminated on the absorber by the i-th mirror (see Fig. 4), it holds that:

$$L_{ai} = \begin{cases} \frac{\pi D}{2} & \text{if } W_{ai} \cos \alpha_i > D \\ D \arcsin \left(\frac{W_{ai}}{D} \right) & \text{if } W_{ai} \cos \alpha_i \leqslant D \end{cases} \qquad (12)$$

for $0 \leqslant i \leqslant 2n$. We must bear in mind that the real value of D must be chosen from among the available standard values for the tubes. Thus, the most reasonable choice for the frontal design is to work with W_a^* to compute CR (see (36)) and, once the design is chosen and the value of W_a^* is fixed, we can choose the D of the tube that best fits the conditions (12), i.e., the one which verifies in most cases $W_{ai} \cos \alpha_i \geqslant D$.

A final modification also needs to be made in the above formulas. This simply involves changing the focal distance, f, in all the above formulas in which it appears by:

$$f' = f + \frac{D}{2} \qquad (13)$$

to take into account the radius of the absorber tube.

3.3. Frontal cosine factor

Finally, it is worth noting that the radiation incident is perpendicular to each mirror-reflector in the frontal plane view once a day. In all other cases, the total radiation on the LFR is directly proportional to the cosine of the angle between the normal to the mirror and the angle of incidence of the sun (θ_i). This factor can be deduced; its value being:
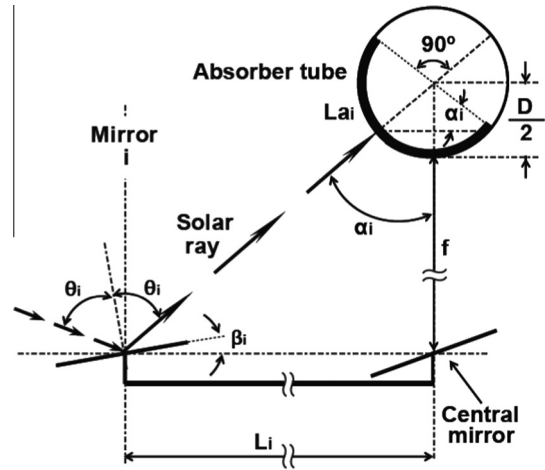

Fig. 4. Cylindrical absorber.

$$\cos \theta_i = \cos \frac{|\theta_f| + \alpha_i}{2}; \quad 0 \leqslant i \leqslant 2n \qquad (14)$$

As can be seen in (14), this factor has a value for each mirror depending on the position of the sun. We shall subsequently see the influence of this factor on the actual radiation that is harnessed.

It should be noted that there is another cosine factor to analyse, namely the one produced when the solar radiation reaches the absorber. In the case of the frontal study, it is straightforward to deduce that the following holds:

$$\cos \theta_{ai} = 1; \quad 0 \leqslant i \leqslant 2n \qquad (15)$$

as the surface of the incident ray is equal to the surface illuminated by the ray.

3.4. Reflection of non-parallel rays

The preceding study is based on the incident light rays being parallel. Actually, this is not true: because of the finite angular size of the sun's disc, the sun's rays reaching the absorber tube are not parallel. Therefore, this consideration affects the focus width and hence the design of the secondary reflector. It specifically affects the calculation of the aperture of the secondary reflector. As already stated, however, this question is not addressed in this paper.

Let us consider the angular diameter of the sun's disc, $\xi \simeq 9.3$ mrad (see Stine and Geyer, 2015). Fig. 5 shows that taking this parameter into consideration means that the focus width, W_{ai}, varies with respect to the value calculated in (10). Obviously, this change also affects L_{ai}. The illuminated area is now increased in two values that we shall call d_i' and d_i''. Their values affect the aperture of the secondary reflector, more than the diameter of the absorbing tube.

The aim is thus to calculate the length of the lower leg of the striped, right-angled triangles in Fig. 5. To determine these distances, we straightforwardly have that:

$$H'_i = \left[\left(L_i - \frac{W}{2}[\cos(\beta_i) \pm \sin(\beta_i)\tan(\alpha_i)] \right)^2 + \left(f + \frac{D}{2} \right)^2 \right]^{1/2};$$
$$0 \leqslant i \leqslant 2n \tag{16}$$

$$H''_i = \left[\left(L_i + \frac{W}{2}[\cos(\beta_i) \pm \sin(\beta_i)\tan(\alpha_i)] \right)^2 + \left(f + \frac{D}{2} \right)^2 \right]^{1/2};$$
$$0 \leqslant i \leqslant 2n \tag{17}$$

The sign $\pm$ must be adopted, once again, according to the following criteria: $-$ for the left side, and $+$ for the right side. Hence, the distances to determine are:

$$d'_i = H'_i \tan\frac{\xi}{2} \tag{18}$$

$$d''_i = H''_i \tan\frac{\xi}{2} \tag{19}$$

These values of d'_i and d''_i are then added to the previously calculated value of W_{ai}. Their influence is thus limited to the frontal study (see Section 6.2); they barely affect the lateral study subsequently presented in Section 6.3.

4. Lateral design

In what follows, we shall perform the lateral study of the LFR. The aim is to compute the optimal relative disposition between the field of primary reflectors and the single absorber tube.

In large-scale LFRs, this study is not usually conducted for two reasons. First of all, the size of the absorber does not permit any configuration to modify its position. Second, the influence of the lateral position can be considered irrelevant in % terms with respect to the total length of the single absorber tube. However, in smaller-sized LFRs, like those analysed in this paper, this is a fundamental study, as we shall subsequently show. In Fig. 6, we describe the notation. We need only take into account the central mirror for this study. Apart from the new variables (which we do not define for the sake of brevity), as before λ is the latitude, θ_z is the zenithal solar angle (with $\theta_z = \theta_l$), f is the distance to
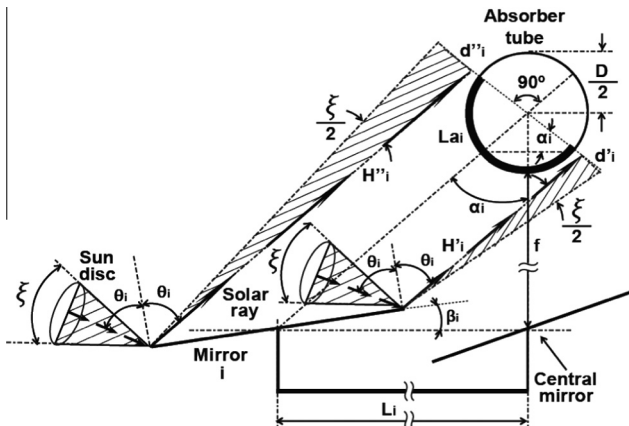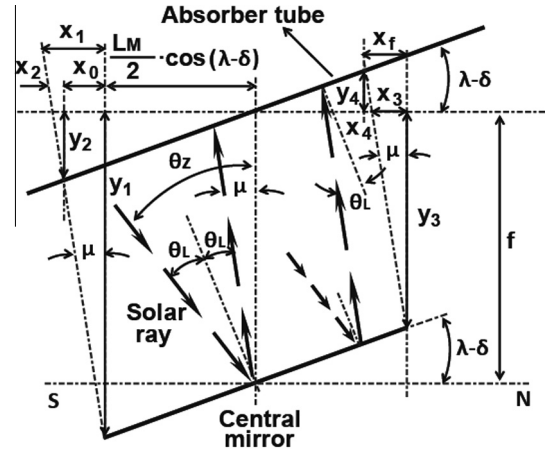
Fig. 5. Reflection of non-parallel rays.

Fig. 6. Definitions used in the lateral design.

the absorber and δ is the declination. L_M represents the length of the mirrors.

Fig. 6 shows the most general configuration possible (C_1). All the particular cases can be deduced from the formulas obtained for this configuration. The following relations between the angles can be verified:

$$\theta_L = \theta_z - \lambda + \delta \tag{20}$$
$$\mu = -\theta_z + 2\lambda - 2\delta \tag{21}$$

and also those between the distances:

$$y_1 = f + \frac{L_M}{2}\sin(\lambda - \delta) \tag{22}$$

$$y_2 = \left[x_0 + \frac{L_M}{2}\cos(\lambda - \delta) \right]\tan(\lambda - \delta) \tag{23}$$

$$y_3 = f - \frac{L_M}{2}\sin(\lambda - \delta) \tag{24}$$

$$y_4 = \left[\frac{L_M}{2}\cos(\lambda - \delta) - x_f \right]\tan(\lambda - \delta) \tag{25}$$

$$x_i = y_i \tan\mu; \quad i = 1, 2, 3, 4 \tag{26}$$

From the above, after some computations, we have that:

$$x_0 = x_1 - x_2 = \frac{f\tan\mu\cos(\lambda - \delta)}{\cos(\lambda - \delta) + \sin(\lambda - \delta)\tan\mu} \tag{27}$$

and

$$x_f = x_3 + x_4 = \frac{f\tan\mu\cos(\lambda - \delta)}{\cos(\lambda - \delta) + \sin(\lambda - \delta)\tan\mu} \tag{28}$$

Thus, $x_0 = x_f$. We also need to consider two lateral cosine factors: one at the mirror and another one at the single absorber tube, which measure the deviation of the incident solar ray from the normal with respect to each of the surfaces. For example, in the configuration shown in Fig. 6, both would be equal to:

$$\cos\theta_L = \cos(\theta_z - \lambda + \delta) \tag{29}$$

which can be seen just by using (20). We proceed to show 12 different configurations for the relative position between the field of primary mirrors and the absorber. Table 1 shows whether the absorber (A) is fixed (F) or movable

(M), the inclination angle of the single absorber tube (tA) and the incidence angle at the single absorber tube (aA). The same data is given for the primary reflectors (Mi).

Position C_1 is inspired by a setting similar to that used in the so-called single axis polar solar tracker. These followers rotate on an axis oriented in the NS direction at an axial inclination equal to the latitude λ of the place, sometimes corrected by means of the declination, δ. Thus, the rotation axis of the system is parallel to the axis of the Earth. Single axis polar solar trackers reach yields of over 96% compared to systems with two axes. This is why we consider this as the basic configuration. In C_1, both A and Mi are movable, but they keep their inclination, $\lambda - \delta$, throughout the day and only move from day to day.

Starting at C_1 and maintaining the same configuration of mirrors, we performed the variations C_2, C_3, C_4 and C_5 employing different fixed inclinations for the absorber. The angle $\zeta = 21.47°$ appears in position C_4. This is defined as the angle θ_z for day $n = 195$ and for solar time $T_S = 12$. We chose these values because they correspond to the day and time of maximum radiation in the whole year. In these 5 positions, the following holds:

$$\theta_L = \theta_z - \lambda + \delta; \quad \mu = -\theta_z + 2\lambda - 2\delta \qquad (30)$$

For position C_6, we also consider A and Mi as movable. In this case, however, they do move throughout the day, because the chosen angle $\left(aA = aMi = \frac{\theta_z}{2}\right)$ depends on the solar time. With this angle, the following holds:

$$\theta_L = \frac{\theta_z}{2}; \quad \mu = 0 \qquad (31)$$

and its value is chosen so that the rays exit Mi perpendicular to the floor. As we shall see in more detail in Section 6, we thus have that the position of A is just above Mi, preventing displacements which are highly detrimental to the design. As before, and starting at C_6, we perform variations maintaining A fixed and employing different inclinations. Observe, for example, that in C_9, the cosine of the angle over A is $\cos 0 = 1$.

Positions C_{10} and C_{11} are inspired by the more classical designs of immovable LFRs. In these, the following holds:

Table 1
Configurations.

	A	tA	aA	Mi	tMi	aMi
C_1	M	$\lambda - \delta$	θ_L	M	$\lambda - \delta$	θ_L
C_2	F	λ	δ	M	$\lambda - \delta$	θ_L
C_3	F	$\lambda/2$	$\delta + \lambda/2$	M	$\lambda - \delta$	θ_L
C_4	F	ζ	$\delta + \lambda - \zeta$	M	$\lambda - \delta$	θ_L
C_5	F	$0°$	μ	M	$\lambda - \delta$	θ_L
C_6	M	$\theta_z/2$	$\theta_z/2$	M	$\theta_z/2$	$\theta_z/2$
C_7	F	λ	λ	M	$\theta_z/2$	$\theta_z/2$
C_8	F	ζ	ζ	M	$\theta_z/2$	$\theta_z/2$
C_9	F	$0°$	$0°$	M	$\theta_z/2$	$\theta_z/2$
C_{10}	F	λ	$\theta_z - \lambda$	F	λ	$\theta_z - \lambda$
C_{11}	F	$0°$	$-\theta_z + 2\lambda$	F	λ	$\theta_z - \lambda$
C_{12}	F	$0°$	θ_z	F	$0°$	θ_z

$$\theta_L = \theta_z - \lambda; \quad \mu = -\theta_z + 2\lambda \qquad (32)$$

Finally, position C_{12} is the most common in large-scale LFRs, with A and Mi being horizontal and fixed. All these configurations shall be tested and we need parameters that allow us to assess their goodness from different points of view. This is what we shall do in the next section.

5. Efficiency of a LFR

To perform a suitable comparative analysis, we must define the relevant parameters to assess each of the suggested configurations. Many types of efficiency are presented in the literature: energy efficiency or optical efficiency, as in for example (see Montes et al., 2014):

$$\eta_{energy}(\%) = \frac{E_{ir}}{DNI \cdot A_{pm}} 100 \qquad (33)$$

$$\eta_{optical}(\%) = \rho_m \frac{Rays_{incident\_receiver}}{Rays_{total}} 100 \qquad (34)$$

where ρ_m represents the reflectivity of the primary mirrors, E_{ir} (W) is the incident energy on the receiver, DNI (W/m²) is the Direct Normal Irradiance, and A_{pm} (m²) the surface area of the primary mirrors. As our study does not include either thermal or energetic aspects, we must accordingly find geometric parameters which characterize both designs.

Different equations are used in the literature (see, for example, Morin et al., 2012; Elmaanaoui and Saifaoui, 2014; Cau and Cocco, 2014) to determine the power absorbed by the absorber tube of an LFR. All of them are made up of the same terms, in general. The total power absorbed from the solar field is thus usually calculated from:

$$Q = DNI \cdot \eta_{opt,0} \cdot x_{field} \cdot CI \cdot IAM \cdot A_m \cdot \eta_{endloss} \qquad (35)$$

where the parameters are: DNI, the Direct Normal Irradiance (Nikitidou et al., 2014), which is the direct irradiance received by a surface that is always held normal to the incoming sun's rays, $\eta_{opt,0}$ is the optical efficiency of the LFR for normal incidence rays to the horizontal ($\theta = 0$) (Nixon et al., 2013), x_{field} is the availability of the solar field; CI is the cleanliness factor, IAM is the incidence angle modifier (Sallaberrya et al., 2014), and describes the variation in optical performances of the LFR for varying incidence angles of rays, A_m is the total area of the LFR, and $\eta_{endloss}$ is the end loss efficiency (Morin et al., 2012), which describes the length of the receiver which is not illuminated by the reflected rays.

In Eq. (35), the IAM contains the variation in the optical performance of a LFR for varying ray incidence angles. However, whereas the IAM generally only considers the frontal design for the case of a large-scale LFR, we consider simultaneously the frontal and the lateral design. In small-scale LFRs, the influence of the lateral design is very important, as we shall see in Section 6. Besides, as this factor is different for each mirror, it will henceforth be denoted as R'_i (see (52)).

5.1. Frontal design

One of the most important and simplest ways of characterizing LFRs is via their concentration ratio (CR) or filling factor (Montes et al., 2014), defined as:

$$CR = \frac{A_{pm}}{A_{abs}} \qquad (36)$$

A_{abs} (m^2) being the area of the single absorber tube and A_{pm} (m^2), the surface area of the primary reflectors, given by:

$$A_{pm} = (2n + 1) \cdot W \cdot L_M \qquad (37)$$
$$A_{abs} = L_{ai} \cdot L_{abs} \qquad (38)$$

where we shall assume, for the frontal design, that the length of the absorber is equal to that of the mirrors:

$$L_{abs} = L_M \qquad (39)$$

This quantity serves as a reference for the increase in the density of radiating flux, given that, in a LFR, the rays are concentrated on a much smaller area than that of the mirrors. However, the incidence angle of the sun is not normal to all the mirrors, so that the true area of the mirrors is not A_{pm}, but in fact it is necessary to compute the projection of each of the mirrors with respect to the incidence of the rays of the sun. This is why some authors (Singh et al., 2010) also use the real concentration ratio (CR_r) defined as:

$$CR_r = \frac{A_{pm\_r}}{A_{abs}} = \frac{\sum_{i=0}^{2n} W \cdot L_M \cdot \cos\theta_i}{A_{abs}} \qquad (40)$$

obtained by summing the concentration contribution of the $2n + 1$ mirrors. In this paper, the assessment of each of the configurations of the frontal design will be carried out using only the parameter (36). The reason for not using (40) is its dependence on the time of the day (see (14)), which complicates the study unnecessarily.

5.2. Lateral design

In order to analyse the lateral design, however, given that the width of the single absorber tube is irrelevant, other parameters must be taken into consideration to achieve a proper assessment of the design. Undoubtedly, due to its influence on the quantity of incident radiation, the most important parameter is the true length of the absorber that is illuminated at each time. In the previous section on the frontal design, for the sake of simplicity we assumed that $L_{abs} = L_M$. However, we shall see that this is not always the most efficient setting.

Moreover, if the absorber is placed such that its endpoints coincide with those of the mirrors, it will have a no illuminated area in most configurations. This is why we shall also have to take into account the relative lateral position of the absorber with respect to the primary mirrors. This factor is important not only to optimize the used radiation, but also from the point of view of the design: if

the illuminated area of the absorber is shifted too far from the vertical of the field of primary reflectors, it may give rise to technically unfeasible configurations.

Thus, we define the left illuminated length of the absorber, l_a^l, as:

$$l_a^l = \frac{x_0 + \frac{L_M}{2}\cos(\lambda - \delta)}{\cos(\lambda - \delta)} \qquad (41)$$

and the right illuminated length of the absorber, l_a^r, as:

$$l_a^r = \frac{\frac{L_M}{2}\cos(\lambda - \delta) - x_f}{\cos(\lambda - \delta)} \qquad (42)$$

both measured from the vertical to the midpoint of the central mirror (see Fig. 5). With these values, we can then compute the total illuminated length:

$$l_a^T = l_a^l + l_a^r \qquad (43)$$

and, from this, we can define a new parameter, the length ratio (LR):

$$LR = \frac{l_a^T}{L_M} \qquad (44)$$

which shall allow us to compare the different configurations. Moreover, l_a^l and l_a^r will also allow us to place A versus Mi in an unequivocal way. We define the deviation with respect to the vertical D_e as:

$$D_e = l_a^l - l_a^r \qquad (45)$$

where the sign of D_e indicates whether it is to the S ($+$) or the N ($-$). Note that this concept has not been considered in such detail till now by any author. The reader can find a short outline of this type of study in Pu and Xia (2011).

5.3. Joint design

In the previous paragraphs, we have seen parameters which allow us to assess the efficiency of the frontal: (36) and (40) and lateral design: (44) and (45) separately. We shall complete this section by presenting a decidedly fundamental aspect: the combination of both studies, the frontal and the lateral design. Both parameters may be combined in a single one as follows:

$$P = \omega_1 CR + \omega_2 LR + \omega_3 D_e \qquad (46)$$

This would have the drawback, however, of having to choose the weight functions, ω_i ($i = 1, 2, 3$), in such a way that is not detrimental to one study versus the other. This is why we consider the most representative parameter to be the resultant, R_i, of the incident radiation, R (with $|R| = 1$). Looking at Fig. 2 again, it can be seen that R has two components: the lateral one, R_l, common to all the mirrors, and the frontal one, R_{fi}, which depends on each mirror. It is straightforward to prove that they satisfy the following equalities:

$$R_l = \frac{\cos \gamma_S \cos \alpha_S}{\cos \gamma_S} = \cos \alpha_S \tag{47}$$

$$R_{fi} = \frac{\cos \gamma_S \sin \alpha_S}{\sin \theta_f}; \quad 0 \leqslant i \leqslant 2n \tag{48}$$

The sum of these two concurrent vectors is:

$$R_i^2 = R_l^2 + R_{fi}^2 + 2R_l R_{fi} \cos \widehat{R_l R_{fi}}; \quad 0 \leqslant i \leqslant 2n \tag{49}$$

If we now take into account the terms introduced by the incidence cosines at each mirror, both the lateral (θ_L) and the frontal cosine (θ_i), we have that:

$$R_l' = R_l \cos \theta_L \tag{50}$$

$$R_{fi}' = R_{fi} \cos \theta_i; \quad 0 \leqslant i \leqslant 2n \tag{51}$$

from which the resultant, R_i' ($0 \leqslant i \leqslant 2n$) is:

$$R_i' = \left[R_l'^2 + R_{fi}'^2 + 2R_l' R_{fi}' \cos \widehat{R_l' R_{fi}'} \right]^{1/2} \tag{52}$$

simply by assuming that the $\cos \widehat{R_l' R_{fi}'}$ is equal at the entry and exit on each mirror.

Remark. As they ignore the lateral study, most authors use the simplified formula:

$$R_i' \simeq R_i^{sim} = R \cos \theta_i; \quad 0 \leqslant i \leqslant 2n \tag{53}$$

In the following section, we shall see how this simplification leads to important design errors in some cases.

6. Numerical simulation

Several ray tracing programs have been reported in the bibliography. In Mills and Morrison (2000), a ray trace model was used in a radiation and thermal model developed in TRNSYS. The model generates optical collection maps in terms of transverse and longitudinal incidence angles. In Grena and Tarquini (2011), a ray-tracing program was written using C++ to predict the optical performance of the system. A software application called TracePro, based on the Monte Carlo ray tracing (MCRT) method, is very known (Xie et al., 2011b; Lin et al., 2013, 2014). TracePro is used to simulate the scattering and diffraction of light. In Monte Carlo ray tracing, scattering and diffraction are treated as random processes. The reader is referred to Garcia et al. (2008), for more information on programs of this kind, which provides a review of the main features of six codes for concentrated solar flux calculation (UHC, DELSOL, HFLCAL, MIRVAL, FIAT LUX and SOLTRACE).

In this study, however, we decided to develop a new code, implemented in Mathematica© to estimate the optical efficiency of the LFR system presented in this paper.

6.1. Programming

Once both the lateral and frontal designs of the LFR have been chosen, θ_f and θ_z must be expressed as functions of the daytime angle, ω, which in turn must be expressed as a function of the legal time, T_L, in order to program the Programmable Logic Control (PLC). It is also well-known that the normal vectors to mirrors at their central points are not parallel to one another. However, the angle made by the normal vectors for two different sun positions is the same for all mirrors. This fact permits rotating all the mirrors of the LFR through the same angle. We accordingly considered two possibilities for the programming:

(i) Always rotating all the mirrors through the same angle, but calibrating the time of the rotation as a function of the day of the year.
(ii) Or rotating the mirrors through an angle that varies with the day of the year, but the same for all the mirrors, at a specified daytime.

In this study, we have chosen the second option, the reason being none other than the choice of a stepper motor. This is a special type of electric motor that moves in increments or steps. The size of the increment is measured in degrees. We shall use increments of 1.8° and, as the motor includes a gear ratio of 100 : 1, which means we can obtain an angle of 0.018° per step.

For the computations of the design, following Spencer (1971) and Duffie and Beckman (2006), we shall consider each day of the year, n_d, one by one, which by means of:

$$\Gamma = (n_d - 1) \frac{2\pi}{365} \tag{54}$$

fixes the daily angle, Γ, and, as a function of this, by means of the following equations:

$$ET = 229.18[0.0000075 + 0.001868 \cos \Gamma - 0.032077 \sin \Gamma \\ - 0.014615 \cos 2\Gamma - 0.04089 \sin 2\Gamma] \tag{55}$$

$$\delta = 0.006918 - 0.399912 \cos \Gamma + 0.070257 \sin \Gamma \\ - 0.006758 \cos 2\Gamma + 0.000907 \sin 2\Gamma - 0.002697 \cos 3\Gamma \\ + 0.001480 \sin 3\Gamma \tag{56}$$

the declination, δ, and the time equation, ET, both constant for each day. Furthermore, the latitude, λ, and the longitude, L_0, are fixed for each position of the LFR. Simply taking into account the relation of α_S and γ_S with ω, given by:

$$\gamma_S = \arcsin[\sin \delta \sin \lambda + \cos \delta \cos \lambda \cos \omega] \tag{57}$$

$$\alpha_S = sign(\omega) \cdot \arccos \left[\frac{\sin \gamma_S \sin \lambda - \sin \delta}{\cos \gamma_S \cos \lambda} \right] \tag{58}$$

and the relation between ω and T_L, given by:

$$T_L = 12 + \omega - \frac{1}{15}(L_0 - L_{UTC}) - \frac{ET}{60} + A_H \tag{59}$$

and by means of elementary computations and substituting in:

$$\theta_f = \arctan \left(\frac{\sin \gamma_S}{\tan \alpha_S} \right) \tag{60}$$

and

$$\theta_l = \arctan\left(\frac{1}{\tan\gamma_S}\right) \Rightarrow \tan\theta_l = \frac{1}{\tan\gamma_S} \quad (61)$$

the following relations are straightforwardly found:

$$\theta_f = f[T_L]; \quad \theta_z = f[T_L] \quad (62)$$

which are required in order to program the PLC (we omit them for the sake of brevity). Another important design factor is the rotation angle adjusting the position of the mirrors. We attempted to find a compromise solution, as frequent rotation usually increases the cost, while doing so sporadically results in large optical errors. Taking into account these considerations, we decided to rotate every 7.5°.

6.2. Frontal design

In the subsequent calculations, we assumed the following data to be fixed: $n_d = 172$ (21 June, Summer Solstice) and the position of the LFR given by $\lambda = 43°17'44''$N and $L = 5°41'3''$W (La Felguera, Asturias, Spain).

For these, we obtained: $\delta = 23.45°$ and $\omega_s = 7.6084$ (h), which corresponds to $T_L = 6.7934$ (h) for the orto. We can now compute the position of the sun at any time of the day, obtaining the plots in Fig. 7.

With these preliminary computations, we can now proceed to the frontal design of the LFR. With the aid of our program, we tried different configurations, solving Eqs. (1) and (2) of the primary field of mirrors. Those authors who follow Mathur's method use the parameter W_a (6) when designing the width of the absorber. Apart from the problem already explained, namely that of being only totally illuminated at one time each day, this parameter depends on the width of the mirrors, W (cm), on the focal height, f (cm), and on the number of mirrors on each side of the central one, n. The influence of these 3 variables creates so many design possibilities, thus increasing the complexity of choosing the optimum one. However, our parameter W_a^* (11) provides the concentration ratio CR (36) with a number of noteworthy properties.

(i) First of all, notice that W_a^* depends almost completely on W for a large range of values of f. In this example, we propose values of $W \in [4, 14]$, which are considered realistic for our design, and the ratio of widths, r_w which has been found to be:

$$r_W = \frac{W}{W_a^*} \simeq 1.115; \quad 100 < f < 200 \quad (63)$$

The reason is that, as i varies with f, there is always a mirror i ($i = 1, \ldots, 2n = 1$) at which the minimum of W_{ai} is reached and this minimum is always the same: W_a^*. Only for values of $f > 200$ and the lowest values of W in [4, 14] does the value of W_a^* increase, though only slightly. We thus we find the following relations
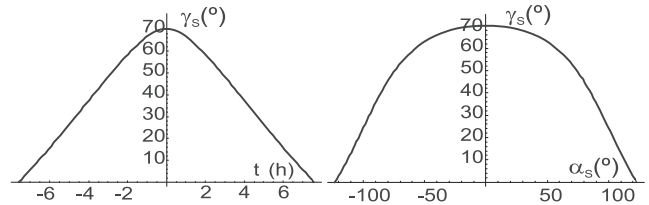

Fig. 7. Position of the sun.

for $\frac{W}{W_a^*}$. The influence is clearly irrelevant and can be discarded for the most common values for the design, assuming $r_w = 1.11$ for all physically meaningful f. A similar argument may be applied for values $f < 100$, though the conflictive values in this case are the largest in the interval [4, 14].

(ii) Secondly, from (36) and (63) it follows straightforwardly that, to all practical effects, CR depends on n for any physically meaningful value of f:

$$CR \simeq r_W(2n + 1) \quad (64)$$

In this example, we propose values of $n \in [8, 16]$, which are considered realistic for our design, the relation we found being (64), with somewhat larger CR, the smaller n is. This is a very important result, as it allows a rapid characterization of any LFR.

(iii) Lastly, the only factor left to consider is the Mirror Field Width, M_{fw}, which logically depends on W, n and, to a much lesser extent, on f. In line with the previous notation:

$$M_{fw} = 2L_n + W \quad (65)$$

First, we have assumed parallel rays; hence, we consider the influence of the finite angular size of the sun's disc to be negligible ($\xi = 0$). Our program in Mathematica© allows us to perform all the desired combinations among the variables rapidly. Considering W (cm) $\in [0, 14]$, $n \in [0, 16]$ and $f = 150$ (cm), we obtained a series of values for M_{fw} (cm). We adjusted these values by means of the Fit command implemented in Mathematica®, obtaining the following approximate function:

$$M_{fw} \simeq 2.70263(W \cdot n) + 0.000483696(W^2 \cdot n^2) \quad (66)$$

The CPU time required by the program to perform the 15·17 combinations was 54.26 sec on a personal computer (Intel Core 2/2.66 GHz) and the r^2 of the 0.9999 approximation.

With the aid of these results, the choice of the frontal design is very simple. All depends solely on technical restrictions. For our study, we show an example of what may most likely be the most common method to start the design by fixing CR, although it is possible to start with different conditions. We show in parenthesis the values we fixed for the example.

(a) Fix an appropriate CR ($CR \sim [28, 32]$).
(b) From (64), deduce the value of n ($n \sim [12, 14]$).

(c)　Fix the max M_{fw} available (max $M_{fw} \sim 200$).
(d)　From (66), compute W ($W \sim [5, 6]$).

Finally, we determined the size of the system, with 25 mirrors ($n = 12$), $W = 6$ (cm) width, with the plane of the absorber placed at $f = 150$ (cm). For this setup, $CR = 27.88$, $M_{fw} = 196.36$ and $W_a^* = 5.37$. The reflective surfaces are commercial grade, 3 (mm) thick and $L_M = 200$ (cm) long. As regards the absorber tube, we chose a diameter $D = 5.34$ (cm) for the reason that, among those available, it is the one which best fits the following condition: $W_{ai} \cos \alpha_i \geqslant D$.

Finally, we verified the negligible influence on the frontal design of the finite angular size of the sun's disc, ξ. If the above calculations are repeated with $\xi = 9.3$ mrad, the following approximate function is obtained:

$$M_{fw} \simeq 2.71112(W \cdot n) + 0.000503639(W^2 \cdot n^2) \qquad (67)$$

As can be seen, the dimensions are now slightly greater than in the previous case. The reason for this is that considering the rays to be non-parallel by including ξ, the separation between mirrors must be somewhat greater in order to avoid the effects of blocking and shading. Nonetheless, the difference is very small. The greatest relative error between the two approaches is 0.45%, the value obtained in the extreme case of $W = 14$ (cm), and $n = 16$.

6.3. Lateral design

We now present the results obtained for the lateral design. Of all the previous configurations, we start by showing the cases C_1, C_6, C_{12} (configuration C_{10} is not analysed because it is very similar to C_{12}). These 3 cases were chosen due to being the most relevant ones. The base case is C_1, inspired by the single axis polar solar tracker, with A and Mi fixed throughout the day, though adjustable from day to day; case C_6 has A and Mi varying throughout the day; case C_{12}, the most common in large-scale LFRs, has A and Mi horizontal and fixed.

Moreover, all of these cases verify that the angles of the absorber and the mirrors are equal (from the lateral point of view): aA = aMi. Hence, we have that $l_a^T = 200$ (cm) for all cases and hence $LR = 1$. What does vary from a configuration to another is the shift relative to the vertical D_e.

In Fig. 8, we show l_a^T, l_a^l and l_a^r for C_1. Analysing the influence of T_S, we see that l_a^l (resp. l_a^r) increases (resp. decreases) from $T_S = 7{:}00$ h (or 17:00 h by symmetry) to 12:00 h, regardless of the day, n_d. The influence of n_d, regardless of T_S, can be seen in Table 3.

In Fig. 9, we show how in C_6, both l_a^l and l_a^r remain constant regardless of the day or time $l_a^l = l_a^r = 100$ (cm).

In case C_{12}, as in C1, l_a^l (resp. l_a^r) increases (resp. decreases) from $T_S = 7{:}00$ h (or 17:00 h by symmetry) to 12:00 h, irrespective of the day, n_d, though now the influence of n_d (see Table 2) is the opposite. Recall that
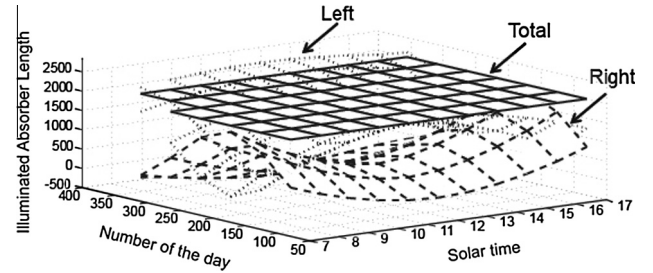

Fig. 8. l_a^T, l_a^l and l_a^r of configuration C_1.

Table 2
Relation W/W_a^*.

W	f			
	250	300	350	400
4	1.109	1.106	1.104	1.101
5	1.113	1.110	1.107	1.105
6	1.115	1.113	1.110	1.108
7	1.115	1.114	1.113	1.111

Table 3
Influence of n_d on D_e.

|	max l_a^l	min l_a^l	max l_a^r	min l_a^l
C_1	356	172	172	356
C_6	cte	cte	cte	cte
C_{12}	172	356	356	172
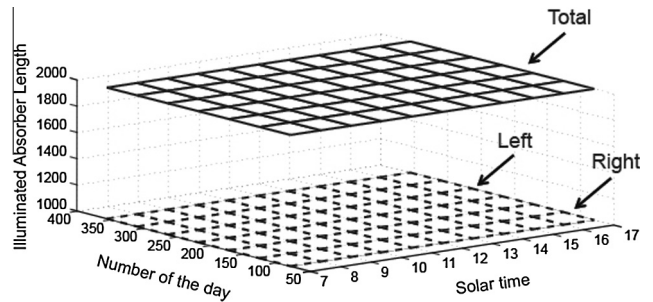
Fig. 9. l_a^T, l_a^l and l_a^r of configuration C_6.

$n_d = 356$ corresponds to the Winter solstice and $n_d = 172$ corresponds to the Summer solstice.

The effect of D_e is perceived more clearly in Figs. 10 and 11, where it is apparent that in order for the absorber to be illuminated, at times it needs to be shifted some metres. Thus, if we only analyse the factors LR and D_e among these configurations (the three with $LR = 1$), C_6 is undoubtedly the best one from the constructive point of view.

Apart from the two parameters LR and D_e already studied, it is also of interest to assess the different configurations from the point of view of the lateral angle of incidence on the mirror: $\cos \theta_L$, due to its effect on the total radiation, R_i'. This factor is shown in Fig. 12 for C_1, C_6 and C_{12}.
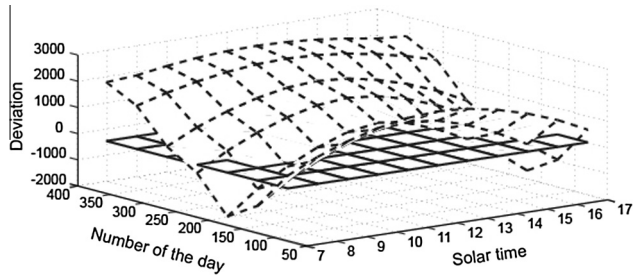
Fig. 10. D_e of configuration C_1.
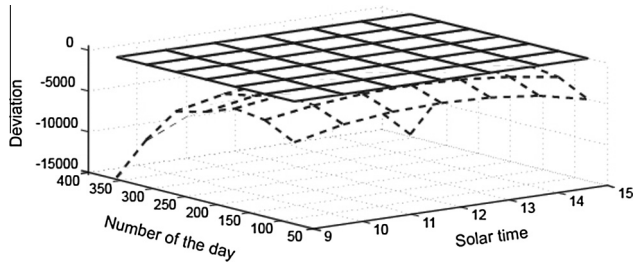
Fig. 11. D_e of configuration C_{12}.
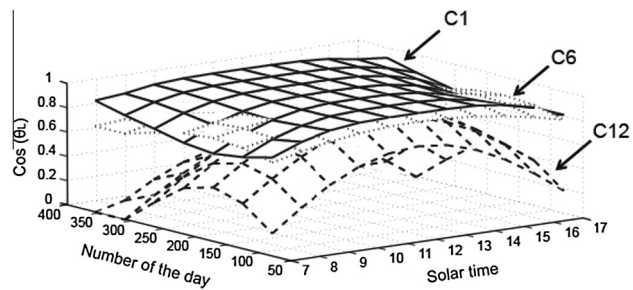
Fig. 12. $\cos\theta_L$ of C_1, C_6, and C_{12}.
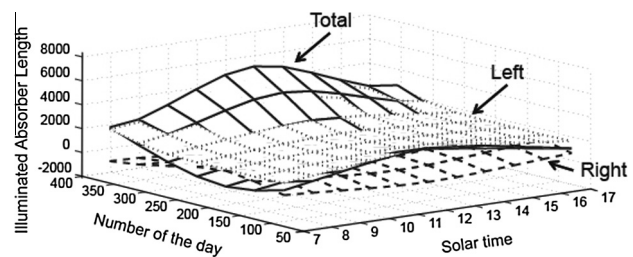
Fig. 13. l_a^T, l_a^l and l_a^r of configuration C_5.

It is clear that the best $\cos\theta_L$ is obtained in all cases for $T_S = 12:00$ (h), regardless of the day, n_d. The influence of n_d, regardless of T_S, can be seen in Table 4.

As for the relative values, the best $\cos\theta_L$ are obtained for C_1, closely followed by C_6, whereas those for C_{12} are much lower. Combining the three factors, LR, D_e and $\cos\theta_L$, we see that the choice of the optimal design clearly lies between C_1 and C_6, with C_{12} being a very bad option, despite this being, surprisingly, the most common large-scale LFR design.

Table 4
Influence of n_d on $\cos\theta_L$.

	max $\cos\theta_L$	min $\cos\theta_L$
C_1	356	172
C_6	172	356
C_{12}	172	356

In the other configurations, the factor LR is variable. We show, as an example (and for the sake of brevity), only configuration C_5 (see Fig. 13). Values of $LR > 1$ are obtained for this configuration, but at the price of such large values of D_e that the design of the LFR is unfeasible from a constructive point of view.

The remaining cases give very similar conclusions to those for C_5.

Among others, the practical implications of the results for the lateral design are those of showing:

– The configuration that has the greatest illuminated absorber length, l_a^T, and hence the one that achieves a greater absorption of energy.
– The days on which the illuminated absorber length is greatest for each configuration. This allows us to know which configuration performs better in the winter months than in the summer months.
– The illuminated absorber length, l_a^T, l_a^r and l_a^l, for each configuration, thus allowing us to know the optimal layout for each configuration.
– The configuration in which the factor $\cos\theta_L$ is closest to 1.

6.4. Joint design

Finally, we show the results obtained when performing the joint design, carrying out the frontal and lateral studies simultaneously. As stated previously, for this joint design we shall use the resultant, R_l'. Moreover, we shall compare the one obtained in this study:

$$R_i' = \left[R_l'^2 + R_{fi}'^2 + 2R_l'R_{fi}' \cos\widehat{R_l'R_{fi}'} \right]^{1/2} \qquad (68)$$

to the simplification used by most other authors:

$$R_i' \simeq R_i^{sim} = R\cos\theta_i; \quad 0 \leqslant i \leqslant 2n \qquad (69)$$

In the presentation of the results, we once again consider configurations C_1, C_6, C_{12}. In Figs. 14–16, the vertical axis represents the differences between the resultants for the simplified studies and the one developed by us:

$$\frac{R_i^{sim} - R_i'}{R_i^{sim}} 100 \qquad (70)$$

which, as can be seen, depend on the mirror and the solar time. Table 5 shows the maximum difference obtained for each configuration and under which conditions.
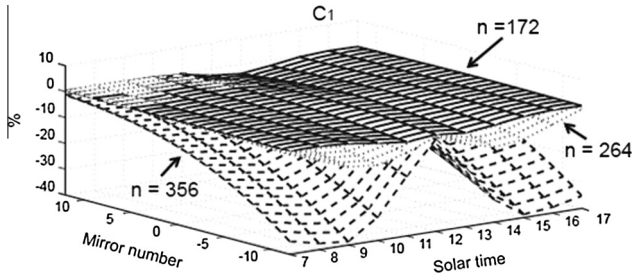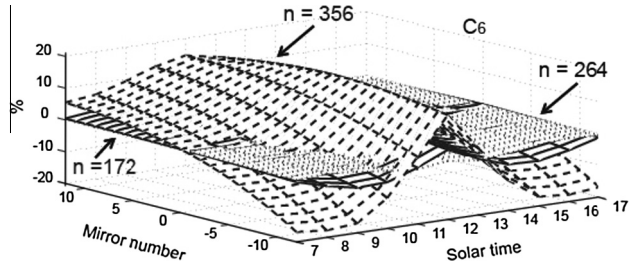
Fig. 14. Influence of the lateral design on C_1.

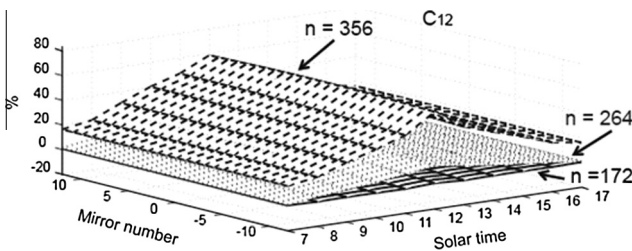Fig. 15. Influence of the lateral design on C_6.

Fig. 16. Influence of the lateral design on C_{12}.

Table 5
Influence of the lateral study on the resultant.

	max%	n_d	T_S	Mirror no.
C_1	−38.69	356	9:00 (15:00)	12 Left (Right)
C_6	−17.86	356	8:00 (16:00)	12 Left (Right)
C_{12}	+60.48	356	12:00	Central

We can see how the classical studies, carried out for large-scale LFRs and which ignore the lateral study, are inadequate for small-scale LFRs, as very large errors can occur.

7. Conclusions

LFR technologies constitute a hot research topic. A number of different LFR systems are currently being developed by different companies, such as Novatec Solar (Germany), Areva Solar (France/USA), MAN/Solar Power Group (Germany), Industrial Solar (Germany), Fera (Italy) and CNIM (France). The LFR has several advantages: it is very useful for medium-temperature range applications (between 100 and 250 °C); it is fabricated with narrow flat mirrors, materials readily and cheaply available on the market; and the planar configuration and the air gap between the adjacent mirrors result in low wind loading on the structure. The first commercial plants are already in service and the previous literature contains several LFR designs.

This paper focuses on an optical and mathematical study, without addressing thermal or economic aspects. The design of a LFR is usually analysed considering a horizontal single absorber tube. In this paper, however, various configurations have been analysed taking into account the lateral view. This study is fundamental when the aim is to obtain the optimal design of a LFR for the Household Sector. The following energy consumptions in households can be identified: space heating, water heating, cooking, space cooling, lighting and electrical appliances. Thermal energy uses correspond to 85% of all household consumption.

Our study has allowed us to show the importance of this lateral design, which, in combination with the frontal design, leads to the optimal solution from the optical point of view. While the frontal design focuses on calculating the number, width and optimal separation of the primary mirrors, as well as the focal height, the lateral design focuses on the relative position between the single absorber tube and the primary reflector. The best design combination has been determined on the basis of new efficiency parameters introduced for the first time in this paper. Furthermore, some of the 12 configurations we present mean that our LFR is actually a hybrid between types I and II, as they allow movement of the individual reflector-rows and that of the reflector-receiver system.

As far as future perspectives are concerned, the subject of the design of the secondary reflector concentrator still remains open. The single absorber tube device plays a very important role in the harnessing of solar energy and the secondary reflector geometry also requires detailed study. It would also be interesting to continue this line of research via the study of thermal behaviour. It should also be noted that, at the time for writing this paper (April 2015), a prototype is being built at the CIFP-Mantenimiento y Servicios a la Producción, in La Felguera, Asturias, Spain, that will enable a comparison with theoretical results.

References

Abbas, R., Montes, M.J., Piera, M., Martínez-Val, J.M., 2012a. Solar radiation concentration features in linear Fresnel reflector arrays. Energy Convers. Manage. 54, 133–144.

Abbas, R., Muñoz, J., Martínez-Val, J.M., 2012b. Steady-state thermal analysis of an innovative receiver for linear Fresnel reflectors. Appl. Energy 92, 503–515.

Cau, G., Cocco, D., 2014. Comparison of medium-size concentrating solar power plants based on parabolic trough and linear Fresnel collectors. Energy Proc. 45, 101–110.

Duffie, J.A., Beckman, W.A., 2006. Solar Engineering of Thermal Processes, third ed. John Wiley & Sons, New York.

Elmaanaoui, Y., Saifaoui, D., 2014. Parametric analysis of end loss efficiency in linear Fresnel reflector. In: Renewable and Sustainable Energy Conference, pp. 104–107.

Fetie, C., 2014. Statistics on Energy Consumption in Households. EUROSTAT, Vienna.

Garcia, P., Ferriere, A., Bezian, J.J., 2008. Codes for solar flux calculation dedicated to central receiver system applications: a comparative review. Sol. Energy 82 (3), 189–197.

Grena, R., Tarquini, P., 2011. Solar linear Fresnel collector using molten nitrates as heat transfer fluid. Energy 36, 1048–1056.

Leutz, R., Suzuki, A., Akisawa, A., Kashiwagi, T., 1999. Design of a nonimaging Fresnel lens for solar concentrators. Sol. Energy 65, 379–387.

Lin, M., Sumathy, K., Dai, Y.J., Wang, R.Z., Chen, Y., 2013. Experimental and theoretical analysis on a linear Fresnel reflector solar collector prototype with V-shaped cavity receiver. Appl. Therm. Eng. 51 (1), 963–972.

Lin, M., Sumathy, K., Dai, Y.J., Zhao, X.K., 2014. Performance investigation on a linear Fresnel lens solar collector using cavity receiver. Sol. Energy 107, 50–62.

Mathur, S.S., Kandpal, T.C., Negi, B.S., 1991a. Optical design and concentration characteristics of linear Fresnel reflector solar concentrators—I. Mirror elements of varying width. Energy Convers. Manage. 31 (3), 205–219.

Mathur, S.S., Kandpal, T.C., Negi, B.S., 1991b. Optical design and concentration characteristics of linear Fresnel reflector solar concentrators—II. Mirror elements of equal width. Energy Convers. Manage. 31 (3), 221–232.

Mills, D., Morrison, G.L., 2000. Compact linear Fresnel reflector solar thermal powerplants. Sol. Energy 68 (3), 263–283.

Montes, M.J., Rubbia, C., Abbas, R., Martínez-Val, J.M., 2014. A comparative analysis of configurations of linear Fresnel collectors for concentrating solar power. Energy 73, 192–203.

Morin, G., Dersch, J., Platzer, W., Eck, M., Häberle, A., 2012. Comparison of linear Fresnel and parabolic trough collector power plants. Sol. Energy 86, 1–12.

Nikitidou, E., Kazantzidis, A., Salamalikis, V., 2014. The aerosol effect on direct normal irradiance in Europe under clear skies. Renew. Energy 68, 475–484.

Nixon, J.D., Davies, P.A., 2012. Cost-exergy optimization of linear Fresnel reflectors. Sol. Energy 86, 147–156.

Nixon, J.D., Dey, P.K., Davies, P.A., 2013. Design of a novel solar thermal collector using a multi-criteria decision-making methodology. J. Clean. Prod. 59, 150–159.

Novatec-Solar, 2015. Technical Data NOVA-1, Puerto Errado. <http://www.novatec-biosol.com/>.

Pu, S., Xia, C., 2011. End-effect of linear Fresnel collectors. In: Proc. Conf. APPEEC, pp. 1–4.

Sallaberrya, F., Pujol-Nadal, R., Martinez-Moll, V., Torres, J.L., 2014. Optical and thermal characterization procedure for a variable geometry concentrator: a standard approach. Renew. Energy 68, 842–852.

Sharma, V.M., Nayak, J.K., Kedare, S.B., 2015. Effects of shading and blocking in linear Fresnel reflector field. Sol. Energy 113, 114–138.

Singh, P.L., Sarviya, R.M., Bhagoria, J.L., 2010. Thermal performance of linear Fresnel reflecting solar concentrator with trapezoidal cavity absorbers. Appl. Energy 87, 541–550.

Spencer, J.W., 1971. Fourier series representation of the position of the sun. Search 2 (5), 172.

Stine, W.B., Geyer, M., 2015. Power From The Sun. <http://www.powerfromthesun.net/book.html>.

Suri, M., Huld, T.A., Dunlop, E.D., Ossenbrink, H.A., 2007. Potential of solar electricity generation in the European Union member states and candidate countries. Sol. Energy 81, 1295–1305, <http://re.jrc.ec.europa/pvgis/>.

Xie, W.T., Dai, Y.J., Wang, R.Z., 2011b. Numerical and experimental analysis of a point focus solar collector using high concentration imaging PMMA Fresnel lens. Energy Convers. Manage. 52, 2417–2426.

Xie, W.T., Dai, Y.J., Wang, R.Z., Sumathy, K., 2011a. Concentrated solar energy applications using Fresnel lenses: a review. Renew. Sustain. Energy Rev. 15, 2588–2606.

Zhai, H., Dai, Y.J., Wu, J.Y., Wang, R.Z., Zhang, L.Y., 2010. Experimental investigation and analysis on a concentrating solar collector using linear Fresnel lens. Energy Convers. Manage. 51, 48–55.